Stable perturbative predictions for isolated photon production with a jet pair at large $m_{j_1j_2}$

Jeppe R. Andersen [a,b] **Andreas Maier** [c,d] **Malina Rosca** [a] **and Giacomo Ruisi** [e]

[a] *Institute for Particle Physics Phenomenology, University of Durham,*
South Road, Durham DH1 3LE, U.K.

[b] *Theoretical Physics Department, CERN,*
1211 Geneva 23, Switzerland

[c] *Institut de Física d'Altes Energies (IFAE), The Barcelona Institute of Science and Technology,*
Campus UAB, 08193 Bellaterra (Barcelona), Spain

[d] *Grup de Física Teòrica, Dept. Física, Universitat Autònoma de Barcelona,*
E-08193 Bellaterra, Barcelona, Spain

[e] *Deutsches Elektronen-Synchrotron DESY,*
Platanenallee 6, 15738 Zeuthen, Germany

E-mail: jeppe.andersen@durham.ac.uk, amaier@ifae.es,
malina.rosca@durham.ac.uk, giacomo.ruisi@desy.de

ABSTRACT: We present the first calculation of the high-energy corrections to the process of isolated photon production in association with two jets. These corrections both stabilise the perturbative behaviour in $m_{j_1j_2}$ and lead to a significantly improved description of data from a recent ATLAS measurement.

Contents

1 Introduction

The impressive efforts of the LHC experiments in achieving increasingly precise measurements of the cross sections of ever rarer Standard Model processes [1] is met by a Herculean effort of achieving similarly precise fixed order predictions from first principles, such that the measurement can be interpreted in terms of the underlying theory. This pursuit has resulted in agreement between prediction and measurement for inclusive processes measured at the LHC which have cross sections spanning more than 9 orders of magnitude. This is true in the region where the notion of a single hard perturbative scale should apply.

Kinematic distributions rather than just the cross sections are often needed when searching for possible signals of new interactions and physics. An example of such a study is a recent measurement from ATLAS of the production of missing transverse momentum and that of a photon, both in association with either at least a single jet or at least two jets [2]. This followed an earlier study [3] of the same process.

The theory predictions confronted with these measurement were met with several problems in describing specifically the normalisation and the kinematic distribution in $m_{j_1 j_2}$, the invariant mass between the two hardest jets. In fact, the description of the recent ATLAS measurement [2] was so poor that the whole dataset on γ+dijets was excluded from the

Photon rapidity	$\|y\| \leq 1.37$ or $1.56 \leq \|y\| \leq 2.37$
Photon energy	$E_\gamma^T > 150\,\text{GeV}$
Jet transverse momentum	$p_T^{\text{jet}} > 100\,\text{GeV}$
Jet rapidity	$\|y^{\text{jet}}\| < 2.5$
Minimum number of jets	2
Jet-photon separation	$\Delta R^{\gamma-\text{jet}} > 0.8$
Phase space cut	$E_T^\gamma > p_T^{j_1}$
Jet definition	anti-k_t, $R = 0.4$

Table 1. Cuts for the 36.1 fb^{-1} sample analysed by ATLAS [3]. Additional cuts were imposed vetoing hadronic activity in an isolation cone around the photon.

analysis on BSM exclusion.[1] The fixed order predictions have large scale dependence and large corrections from NLO to NNLO [4] and slow numerical convergence for large $m_{j_1 j_2}$. In fact, the NNLO results converge only up to $m_{j_1 j_2}$ around 1TeV, whereas the recent measurement by ATLAS [2] extends to 8.2TeV. The shower-based merging of NLO-matched samples [5], while numerically stable, fails to describe the distribution at large $m_{j_1 j_2}$.

In the current study we will calculate the predictions for the photon+dijets measurements in reference [2] and demonstrate that the all-order resummation of logarithms relevant at large $m_{j_1 j_2}$ obtains a stable, precise and accurate prediction of data, where fixed next-to-leading order and other predictions struggle to describe the distribution.

Section 2 will detail the relevant components of the measurement for this study. Section 3 explains the challenges posed to fixed order for the current measurement. The resummation leading to perturbative stability is introduced in section 4, and the comparison to data is presented in section 5. Finally, the conclusions are presented in section 6. The appendices A–D contain further discussions of the resummation and of fixed order results using an alternative choice of factorisation and renormalisation scale.

2 ATLAS 13 TeV measurements of photon+Dijets and the status of predictions

The production of prompt photons in association with jets at the LHC energy of 13TeV has been studied in two ATLAS papers with an integrated luminosity of 36.1 fb^{-1} [3] and 140 fb^{-1} [2] focusing on a very inclusive and a very exclusive measurement respectively. The comparison with NNLO[2] [4] focuses on the "direct enriched" sample of the inclusive measurement with the cuts listed in table 1. The hard cut on the photon and the requirement on photon isolation ensure this sample is dominated by contributions where the photon is produced directly from the hard process, rather than through the fragmentation of the produced hard partons. This study includes only central jets ($|y^{\text{jet}}| < 2.5$), and the cuts on the transverse energies and momenta of jets and photons are slightly different than for the measurement to be studied later. Most importantly, this study is *inclusive* in the number

---

[1]The description of the $m_{j_1 j_2}$ spectrum for Z+dijets is also poor.
[2]NNLO in the QCD contribution, see later for a discussion of the electro-weak component.

Photon rapidity	$|y| \leq 1.37$ or $1.52 \leq |y| \leq 2.47$
Leading photon p_T	$> 160\,\mathrm{GeV}$
p_T^{recoil}	$> 200\,\mathrm{GeV}$
Leading jet p_T	$> 80\,\mathrm{GeV}$
Sub-leading jet p_T	$> 50\,\mathrm{GeV}$
Leading jet $|y|$	< 4.4
Sub-leading jet $|y|$	< 4.4
Dijet invariant mass $m_{j_1 j_2}$	$> 200\,\mathrm{GeV}$
$|\Delta y_{j_1 j_2}|$	> 1
Jets with rapidity in-between hardest two	None with $p_T > 30\,\mathrm{GeV}$
Jet definition	anti-k_t, $R = 0.4$

Table 2. Cuts for the analysis reported in reference [2]. The analysis is implemented in Rivet [18].

of jets (no central jet veto as in [2]). However, we can draw some conclusions which will be of relevance for the detailed study of the more recent measurement [2] to follow. The first conclusion already mentioned in [3] is that for this process even the NLO-matched and multi-jet merged approach detailed in [5] describes data only for $m_{j_1 j_2} < 1\mathrm{TeV}$ (see figure 9 of [3]).

The second set of observations of relevance for the later studies are from the presentation of the first full NNLO calculation [4] for this process. First, we note (figure 6 of reference [4]) that pure NLO and MEPS@NLO have very different shapes in $m_{j_1 j_2}$ even though this is an inclusive two-jet observable. This is of course permitted, even if the calculation share the same $\alpha_s^2 \alpha$ and $\alpha_s^3 \alpha$ terms. Secondly, the NNLO corrections can lower the normalisation of the cross section obtained from NLO by roughly 15%, depending on the scale choice. The NNLO calculation [4] studied the similar scale choices of $E_\perp^\gamma$ and H_T (the scalar sum of the transverse momenta of the photon and of the two hardest jets). It would be interesting to understand further whether this change in normalisation from NLO to NNLO is related to the logarithmic corrections from small-cone isolation [6–8] or to super-leading logarithms and other higher-order effects [9–17]. While the NLO calculation is numerically stable for this inclusive measurement across the range of $m_{j_1 j_2}$ studied up to 4TeV, the NNLO calculation displays large numerical variations in the bins beyond 1TeV. The authors identify the cause of the lack of numerical convergence as being due to the large cancellations between the various components of the NNLO calculation [4].

The recent ATLAS study [2] used 140fb^{-1} of data to analyse photon production in association with dijets within the cuts listed in table 2. A few differences in the cuts compared to the earlier ATLAS analysis are worth pointing out, since they will impact the perturbative predictions significantly. While the cuts on the transverse momentum of the photon and of the jets are changed only slightly, the rapidities of the jets in reference [2] can extend to 4.4, allowing for much larger inter-jet rapidities and larger $m_{j_1 j_2}$. The most important difference though is the requirement of the absence of a third jet above 30 GeV with a rapidity in-between the two hardest jets, which are also required to be at least one unit of rapidity apart. While the minimum rapidity separation requirement is modest, the rapidity veto removes the contribution from a third jet in-between the two hardest jets from the

corresponding inclusive prediction. It therefore introduces a perturbative effect proportional to $\alpha_s|\Delta y_{j_1 j_2}|$ relative to a setup similar to the perturbative calculation [4], which is relevant for the inclusive measurement [3].

The following three kinematic distributions were reported by ATLAS (see figure 12 of [2]):

1. $d\sigma/dp_T^\gamma$ in 11 bins 200 GeV $< p_T^\gamma <$ 2600 GeV

2. $d\sigma/dm_{j_1 j_2}$ in 14 bins for 200 GeV $< m_{j_1 j_2} <$ 8200 GeV

3. $d\sigma/d\Delta\phi_{j_1 j_2}$ in 20 bins for $-1 < \Delta\phi_{j_1 j_2}/\pi < 1$

In line with the conclusions from the inclusive measurement in reference [3], the prediction from MEPS@NLO [5] is uniformly 15%-20% high for the predictions for $d\sigma/dp_T^\gamma$ and $d\sigma/d\Delta\phi_{j_1 j_2}$ of reference [2], whereas even the shape of $d\sigma/dm_{j_1 j_2}$ is very poorly described (see figure 12 of [2]) with a systematically increasing deviation from data for increasing $m_{j_1 j_2}$. This very poor Standard Model description of the spectrum meant that the data on photon+dijets had to be disregarded from the BSM search and exclusion study in reference [2].

We will in the next section investigate the fixed order predictions, and in section 4 demonstrate how stable predictions can be obtained using a purely perturbative approach.

3 Investigating fixed order predictions

The process $pp \to \gamma j j$ has at Born level both a QCD $\alpha_s^2\alpha$ and an electro-weak α^3 component, and both are equally relevant at large $m_{j_1 j_2}$. Our primary focus will be on the QCD component, since the perturbative corrections to the electro-weak component are better behaved and controlled. The interference between the QCD and electro-weak (EW) process will be suppressed by colour effects just as for the QCDxEW effects in $pp \to hjj$ [19–21].

We will start the perturbative investigation by calculating the QCD dominated contribution to $pp \to \gamma j j$ at $\alpha_s^2\alpha$ (Born level) and up to $\alpha_s^3\alpha$ (next-to-leading order), both using the conventional choice for renormalisation and factorisation scale of $\hat{H}_T/2$ (half the scalar sum of the transverse momenta of the final state particles). A conventional 7-point scale variation with a factor of 2 is employed. We will focus our attention solely on the distribution $d\sigma/dm_{j_1 j_2}$, since it will cleanly illustrate the issues which arise. The fixed order calculations of the QCD process are performed using Sherpa 2.2.16 [22] and OpenLoops [23], with the analysis implemented in Rivet 4 [18], employing the anti-k_t [24] jet-algorithm implemented in FastJet [25]. For all the predictions presented in this study we use the NNPDF3.1 [26] set provided by LHAPDF [27]. We have checked that the difference to PDF4LHC21 [28] is insignificant at small $m_{j_1 j_2}$ and grows to 10% in the last bin in the $m_{j_1 j_2}$-distribution.

Figure 1 shows the Born level prediction of $d\sigma/dm_{j_1 j_2}$ including scale variation in red and the NLO prediction in blue. While the Born level prediction remains physical for all $m_{j_1 j_2}$, the central prediction at NLO turns small or even negative around 3TeV, and the width of the scale variation band increases uniformly with $m_{j_1 j_2}$. There is overlap between the scale variation bands at LO and NLO only for small $m_{j_1 j_2} < 800$GeV.

It may at first be hard to reconcile the stability found at NLO in reference [4] with the result in figure 1. However, several differences are worth highlighting. Firstly, the
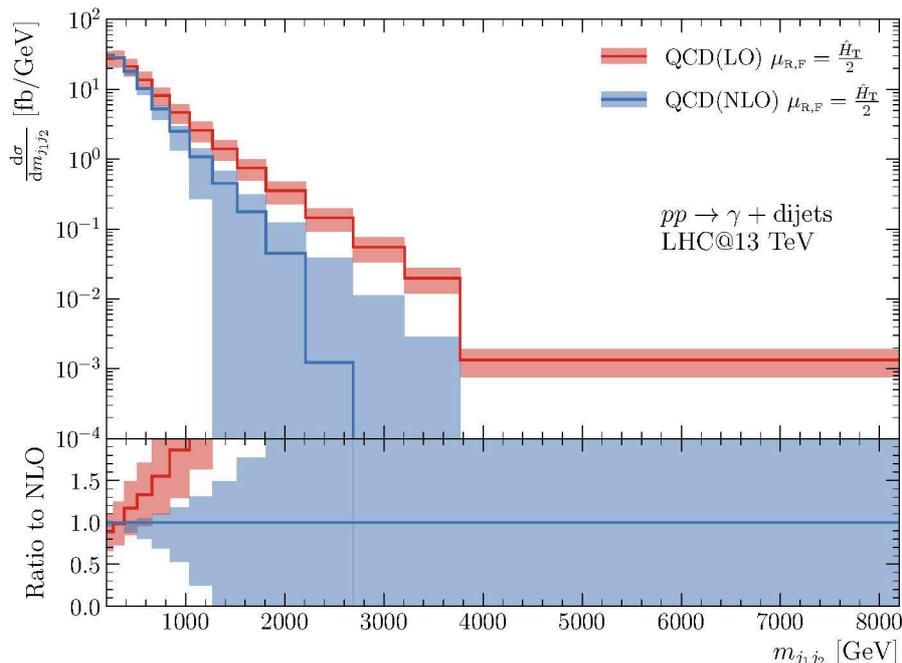
Figure 1. $d\sigma/dm_{j_1j_2}$ for LO and NLO for $pp \to \gamma jj(\alpha_s^2\alpha)$ with central scale choice $\mu_R = \mu_F = \hat{H}_T/2$ and a standard 7-point scale variation.

central jet veto in the current analysis has removed a large positive contribution of the form $\alpha_s\Delta y \sim \alpha_s \log(m_{j_1j_2}/p_t)$ from the inclusive setup in [3, 4]. Secondly, using the scale H_T results in the upper scale variation limit, which stays positive even for the jet vetoed cross section up to the 4TeV limit relevant for the inclusive studies of [3, 4]. The cross section is of course completely determined by the behaviour in the first few bins, and the fact that its value turns negative or close to zero for $m_{j_1j_2} > 4$TeV is a problem only for that particular distribution, not even for the other two distributions studied.

Why would we then choose $\hat{H}_T/2$ rather than $\hat{H}_T$ as the central scale for the calculations reported here and in later sections? $\hat{H}_T/2$ is a standard scale choice used in the predictions for vector boson production in association with jets [29–32]. Choosing $\hat{H}_T$ does not solve the problem, it just pushes both the explosion of the size of the scale variation and the negativity to larger $m_{j_1j_2}$. As such, choosing any specific multiple of $\hat{H}_T$ to make LO and NLO similar would seem like a perturbative fine tuning rather than a useful choice for a true prediction. Even the calculation at NNLO [4] presents two similar scale choices (H_T and E_γ^T) which lead to different conclusions about the size of the NNLO corrections.[3] As mentioned in section 2, even the NNLO corrections [4] on the total cross section were reported to be up to 15% compared to NLO.

In conclusion, we have identified issues of perturbative instability for large $m_{j_1j_2}$ for the next-to-leading order predictions relevant for the measurement in reference [2].

---

[3]It would be interesting if an analysis as the one done in reference [33] could identify a reasonable dynamic scale across phase space.
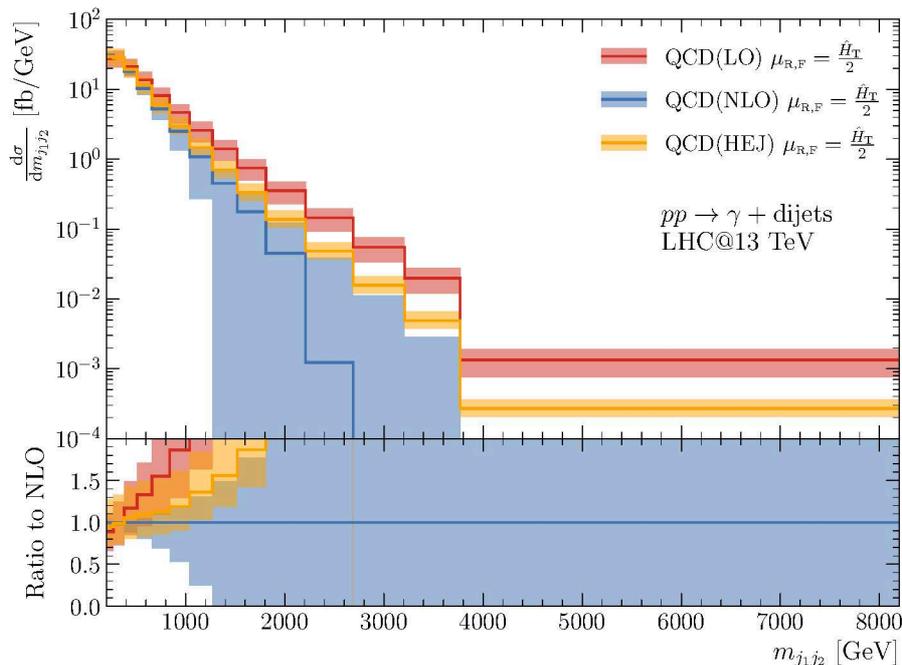
Figure 2. $d\sigma/dm_{j_1 j_2}$ for pure QCD LO, NLO and HEJ matched to NLO.

4 Establishing perturbative stability at large partonic invariant mass

Having identified issues in the perturbative series at large $m_{j_1 j_2}$, and noting that $m_{j_1 j_2} < \sqrt{s}$ (such that large $m_{j_1 j_2}$ means large $\sqrt{s}$), it becomes interesting to investigate the predictions obtained within a perturbative approach which systematically addresses the perturbative logarithms arising in s. These so-called high energy logarithms can be resummed using the BFKL [34–37] equation. However, this approach is *inclusive* in any emission, and therefore not directly suitable for a measurement employing a central jet veto.

We will use here the framework of High Energy Jets (HEJ). This framework captures the same logarithms from full QCD as BFKL, but the all-order resummation is constructed by an explicit sum over the (numerical) phase space integral over each multiplicity, and it is therefore possible to use standard jet-algorithms and analyses. Indeed, the same packages mentioned in the discussion for the fixed-order calculations in section 3 are used for the analyses of the results obtained with HEJ. Furthermore, the amplitudes in HEJ differ in several ways from those of BFKL in retaining the gauge-invariance, crossing symmetry and Lorentz invariance of full QCD, see reference [38] for details.

This is the first study of photon production in association with dijets with HEJ, and several new components had to be calculated. We include selected sub-leading logarithmic corrections, denoting the accuracy as LL^+. The difference between LL and LL^+ amounts to roughly 20% almost uniformly across $m_{j_1 j_2}$. We match the cross section multiplicatively to NLO, observing a small matching correction of 0.5% for the central scale choice and a surprisingly good agreement for $d\sigma/dm_{j_1 j_2}$ between NLO and the NLO-truncated resummation. Further details can be found in appendices A–B.

Figure 2 shows in orange the result for $d\sigma/dm_{j_1j_2}$ obtained with the all-order summation and matching procedure for this process. The result is in-between the fixed order curves for LO and NLO, and the scale variation is reduced compared to that found at LO. The results all agree within scale variations at small $m_{j_1j_2}$, but diverge from around 1TeV. Compared to the result at LO, the distribution falls of slightly steeper. This fall-off and the shape of the distribution is directly controlled by the resummation. In fact, the unphysical limiting behaviour of the NLO calculation can be understood from the NLO expansion of the resummation: having removed much of the real emission contribution with a central jet veto, the influence of the virtual corrections is seen immediately. The high energy limit of the virtual corrections is dominated by a term $\propto \alpha_s \log(s/t)$, so it is hardly surprising that ultimately the cross section can become very small or even negative. This divergent behaviour at NLO is regulated by the all-order resummation: the universal logarithmic virtual corrections are summed to an exponential and the real emission contributions calculated order by order with universal effective vertices; but the order-by-order expansion of the resummation still displays the same divergent behaviour seen at full fixed-order NLO, see appendix B for further details.

In conclusion, we have demonstrated that addressing the terms of order $\alpha_s \log(s)$ to all orders in the perturbation theory has regulated the divergent behaviour, which showed up at NLO.[4] Obviously, the next question is how the resummed prediction compares then to data.

5 Comparison to data

Before comparing directly to data, the electro-weak component has to be added to the QCD component of the previous sections. The electro-weak here was calculated with VBFNLO 3.0 [39, 40]. The NLO QCD corrections to the EW process have a very different logarithmic structure from that of the QCD dominated process for similar reasons as those observed for Higgs production in association with dijets [41]. We observe that compared to LO the QCD NLO correction to the electro-weak process is small at small $m_{j_1j_2}$, and from around 1TeV rises uniformly to 20% in the bin of largest $m_{j_1j_2}$.

Figure 3 shows the QCD and the electroweak component of $pp \to \gamma jj$ as a function of $m_{j_1j_2}$. The QCD component dominates for $m_{j_1j_2} \leq 3$TeV dropping to 30% of the cross section in the last bin. The impact of any variation in the prediction of the QCD component will therefore decrease with increasing $m_{j_1j_2}$.

With that in mind we compare in figure 4 data directly to the sum of the electro-weak component and the predictions of the QCD components calculated at NLO (blue) and with HEJ (red). Since the last two bins span half the range, and in order to emphasise the region dominated by the QCD process we present on figure 4 (left) the region $m_{j_1j_2} < 3.2$TeV and on figure 4 (right) the full range. We note that since the prediction from HEJ inherits the normalisation from NLO it is overshooting the cross section by around 30%. The HEJ prediction can easily be expanded to $\alpha_s^4\alpha$, so could have been matched to NNLO accuracy,

---

[4]To further identify the high-energy logarithmic terms as the cause of problems for the fixed-order expansion, we also calculate in appendix D the fixed-order contributions using the factorisation and renormalisation scale $m_{j_1j_2}$ (such that $\log(s/\mu_r^2)$ does not grow). While the series appears more stable, the central scale choice leads to results which are at the edge of the scale variance band. This strongly suggests that scale variance is not a trustworthy indicator for missing higher order terms.
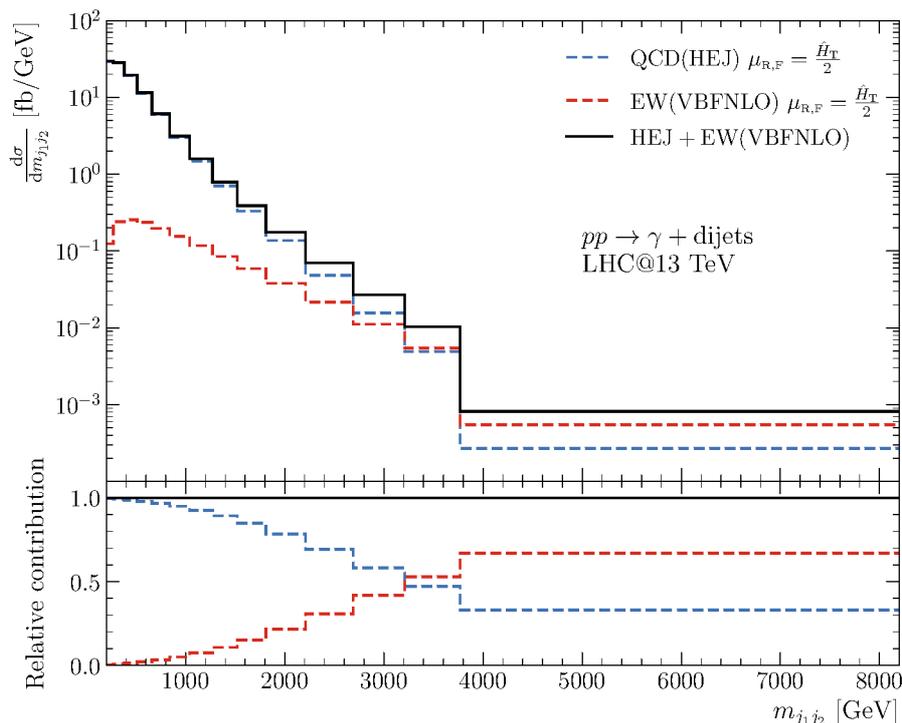
Figure 3. $d\sigma/dm_{j_1 j_2}$ for the QCD component (calculated with HEJ) and the electro-weak component (calculated with VBFNLO). The process is dominated by the QCD contribution until around 3TeV.
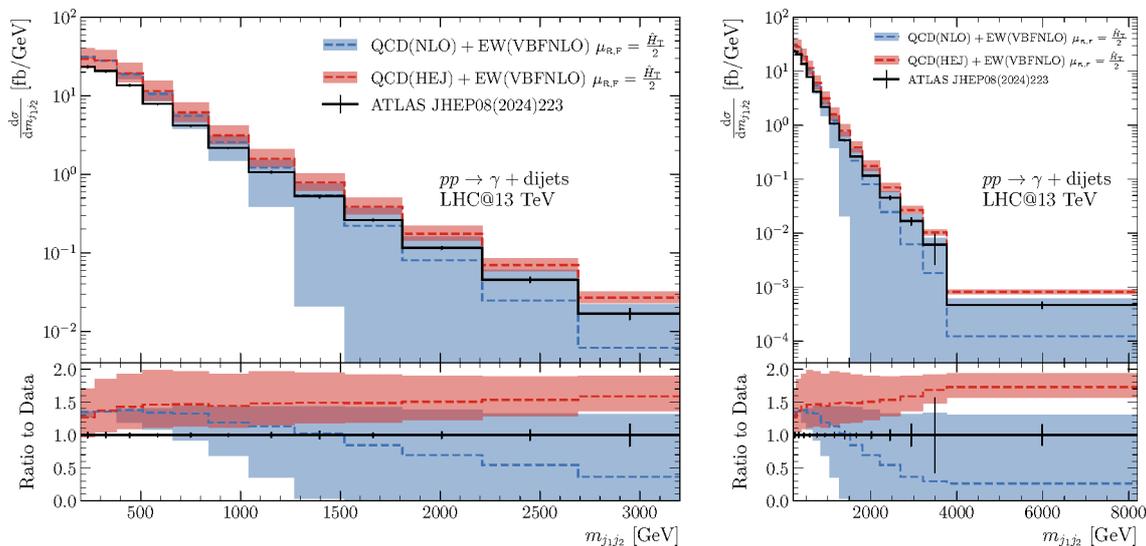

Figure 4. $d\sigma/dm_{j_1 j_2}$ for NLO QCD+EW(VBFNLO), HEJ+EW(VBFNLO) and data. The prediction for HEJ is matched to NLO.

Prediction	Scaling factor σ	χ^2_σ/dof	Scaling factor $\chi^2_{\min}$	$\chi^2_{\min}/dof$
QCD(NLO)+EW(NLO)	0.755	16.3	0.810	14.3
MEPS@NLO	0.832	5.03	0.779	3.18
QCD(HEJ)+EW(NLO)	0.716	1.25	0.689	0.670

Table 3. Scaling factors for normalising the cross section and for minimising χ^2 in the description of the distribution.

had this calculation been performed for the current measurement. Given the observation of the NNLO corrections [4] for the earlier more inclusive measurement [3] it is conceivable that the NNLO calculation would correct the normalisation.

The shape of the distribution with the combined prediction from HEJ and VBFNLO is in very good agreement with data. To illustrate this we investigate two methods for setting the normalisation of both the NLO and HEJ predictions. One can normalise the predictions to the data (equivalent to comparing $1/\sigma \, \mathrm{d}\sigma/\mathrm{d}m_{j_1j_2}$), or float the normalisation to minimise the χ^2. In table 3 we list in the first column the scaling factors needed to normalise to data for QCD(NLO)+EW(NLO), QCD(HEJ)+EW(NLO) and the MEPS@NLO [5] prediction included in the ATLAS study [2]. The fact that the scaling factors for NLO(QCD+EW) and HEJ +EW(NLO) are similar (0.755 and 0.716 respectively) is a result of matching HEJ to the perturbative series at NLO. In other words, the scaling factor for HEJ is roughly the same with which NLO overshoots data. The χ^2-values obtained for the central predictions with this normalisation are 16.3 NLO(QCD+EW), 5.03 (MEPS@NLO) and 1.25 (HEJ+EW) respectively.[5]

Next, we investigate the choice of normalising each prediction to minimise the χ^2. The scaling factors obtained with this method are listed in the third column of table 3. The pair of scaling factors and χ^2 values are (0.810,14.3) (NLO(QCD+EW)), (0.779,3.18) (MEPS@NLO) and (0.689,0.670) (HEJ+EW) respectively.

The scaled predictions are presented in figure 5.[6] As is evident from there, the systematic treatment of the high-energy logarithms results in an excellent description of the distribution. Judging from the findings in reference [4], it is possible that the NNLO corrections on the NLO result would be a more accurate prediction of the normalisation, which could then be used for perturbative matching.

We note that the trends and conclusions are completely in line with those found in reference [2] for Z+dijets. Compared to data, the normalisation for the predictions for $pp \to \gamma jj$ is a little higher than those for $pp \to Zjj$. But the prediction for the shape of $\mathrm{d}\sigma/\mathrm{d}m_{j_1j_2}$ from the NLO matched and parton-shower merged MEPS@NLO fails to describe the shape for both Z and γ production in association with dijets. The systematic treatment in HEJ of the large logarithmic at increasing $m_{j_1j_2}$ improves the description for all the cases studied.

---

[5]Only the experimental uncertainty is used for calculating the χ^2, the scale variation around the central prediction is not used (it is not symmetric and certainly not Gaussian distributed).

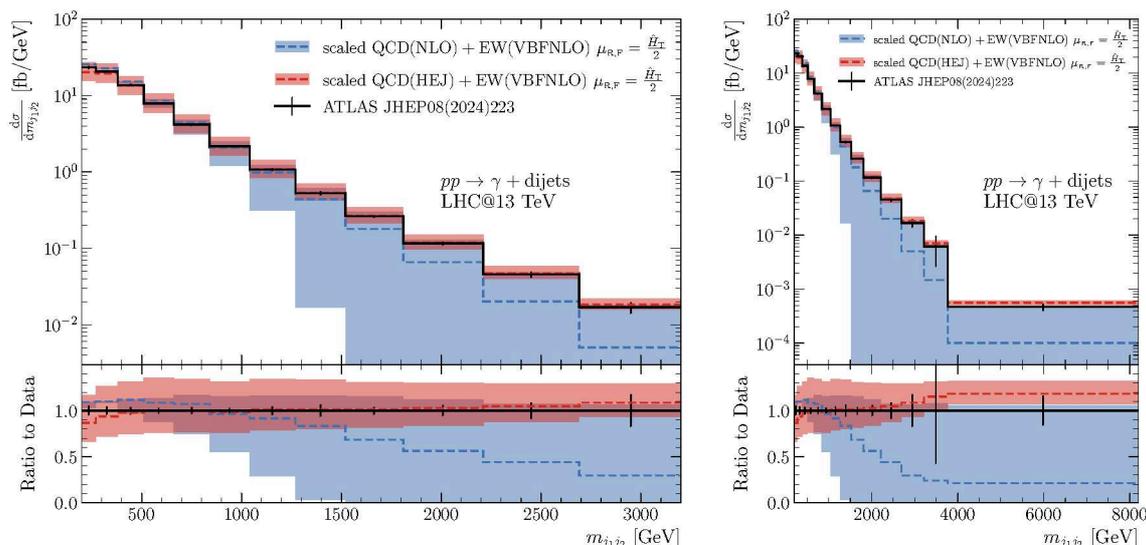[6]Figure 8 in appendix C contains the figures with the result from reference [2] of MEPS@NLO included.

Figure 5. $d\sigma/dm_{j_1j_2}$ for scaled NLO, HEJ and data, see table 3 for the scaling factors and χ^2/dof obtained.

6 Conclusions

We identified issues in the fixed order predictions for a recent ATLAS measurement [2] as arising from high-energy logarithms. These issues are solved in the systematic all-order logarithmic treatment within HEJ. The stabilised perturbative prediction give a good description of the distribution $d\sigma/dm_{j_1j_2}$ which was not well described by predictions available until now. We note that these results are based on first-principle purely perturbative predictions without any tuning.

The analysis [2] thereby joins another recent measurement from ATLAS [42] indicating the appearance of high energy logarithmic effects in analyses relevant for standard perturbative observables and for BSM search and exclusions, in particular for the phase space regions normally considered for studies of vector boson fusion and vector boson scattering.

The issues identified in this study are also present in the channels of Z+jets and W+jets considered in reference [2]. These processes will be the focus of further studies.

The predictions presented in the current study were obtained using the public release of HEJ 2.3 available at http://hej.hepforge.org.

Acknowledgments

A Components for the high energy resummation of γ+Dijets

The calculation of the components needed for the high-energy corrections to the process $pp \to \gamma jj$ follows from the approaches outlined for $pp \to Z/\gamma^* jj$ [45] and $pp \to Wjj$ [38] (in both cases a decay of the vector boson to charged fermions is implied). The outline of the calculation will be described in this appendix. Compared to the previous studies, the calculation presented here is simplified by the photon being on-shell, so instead of having a propagator and decay current the amplitude will have just a polarisation vector. The advancements compared to the previous studies involving γ^*/Z+jets are that all the next-to-leading logarithmic real-emission components equivalent to those derived earlier for $pp \to Wjj$ are now applied in a process where quantum interference between a photon emission from each of the components is significant and needs to be taken into account in order to get a satisfactory description of the full amplitude [45]. This is particularly true at the very large $m_{j_1 j_2}$ considered in this study, where the di-quark perturbative initial state contributes significantly. The interference of photon emission from any of quark lines in the process leads to interferences in the resummation over several different transverse momenta. This is described in reference [45], but is further complicated by the additional NLL components taken into account leading to up to 3 quark lines with possible photon emission in the $pp \to \gamma+4$j component. The full details of both this calculation for $pp \to \gamma jj$ and that for $pp \to (Z \to)\nu\nu$+dijets will appear in future publication. The process of photon production in association with dijets is available in the version 2.3 release of HEJ available at [57].

A.1 Impact currents and central emission

The appearance of all-order logarithmic $\log(s/t)$ corrections in the perturbative description of $pp \to \gamma jj$ follows identical arguments to those for $pp \to jj$ [34–37, 46–48]. Firstly, one observes that for fixed transverse momenta and $s_{cd}, s_{d\gamma} \gg |s_{bd}|$ the scattering amplitude for $q_a g_b \to q_c g_d \gamma$ calculated at Born level factorises into two components depending on the momenta of (p_a, p_c, p_γ) and (p_b, p_d) only, contracted in colour and momentum space as if

they exchanged a single gluon:

$$\xrightarrow[\substack{s_{cd},s_{d\gamma}\gg|s_{bd}| \\ \text{fixed } p_t}]{} \tag{A.1}$$
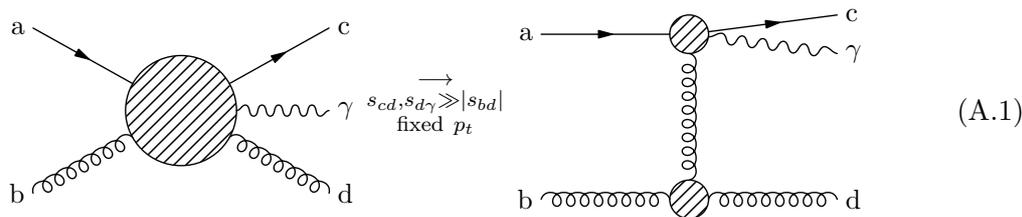
The requirement of fixed transverse momenta is to ensure the large invariant masses are reached by a hierarchy in positive and negative light-cone momenta, rather than by increasing transverse momenta.

Within the formalism of BFKL [34–36] the *impact factor* of (b,d) would depend on *transverse* momenta only [47, 48]. In contrast, the factorised formalism developed for HEJ [49–51] maintains full momentum dependence, which ensures the analytic properties of the amplitude of crossing symmetry, gauge invariance and Lorentz invariance can be (and are) maintained. Apart from the appeal of maintaining the analytic properties of the scattering amplitude, the matching corrections are smaller than for BFKL because of the much milder approximations. Details of how the components are extracted from the full amplitude can be found in references [38, 45, 49].

The crucial conjecture [34–37] for $pp \to jj$ is that the logarithmic $\log(s/t)$-component of the real part of the virtual corrections can be obtained to all orders by a simple substitution of the t-channel gluon propagator between the impact factors. This conjecture has been verified directly up to next-to-leading logarithmic accuracy for full next-to-next-to-leading order amplitudes [52]. This means that the leading behaviour in the *Regge kinematic limit* can be predicted to all orders. In fact, not only processes dominated by the spin-1 colour octet exchange *Reggeize* in this way, but so do processes with an exchange of quark quantum numbers [53].

The amplitudes for real emission corrections also simplify in the *multi-Regge kinematic limit* (MRK) of increasing invariant mass between all of the final state coloured particles (again with fixed transverse momentum) [48]. In the MRK limit, each additional gluon emitted leads to a factor of the *Lipatov vertex* $C_A \alpha_s / (\pi k_{i,\perp}^2)$ in the square of the amplitude. This factorisation is illustrated in equation (A.2):

$$\xrightarrow[\substack{s_{cd},s_{\gamma d}\gg s_{1d}\gg|s_{bd}| \\ \text{fixed } p_t}]{} \tag{A.2}$$
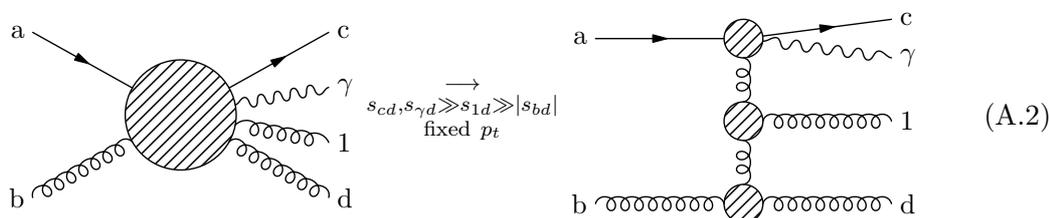
In HEJ, the central jet vertex is a Lorentz tensor [49] such that in the soft limit $k_{i,\perp} \to 0$ the effect on the square of the scattering amplitude tends to the simpler Lipatov vertex [51]. However, the full tensor structure is of course necessary in order to fulfil the Ward identity.

For fixed s_{cd}, the phase space integral over gluon 1 leads to logarithmic corrections. The infrared pole cancels between the contribution from the real emission and that of the

virtual corrections, leading to a finite corrections which crucially has logarithmic contributions from both real and virtual corrections. This feature persists in the MRK limit to all orders in the coupling.

A.2 The quasi multi-Regge kinematic limit

The factorisation of amplitudes into sub-components of less analytic complexity extends beyond leading logarithmic accuracy. Specifically, factorised amplitudes can be constructed which describe correctly the situation when the restriction in equation (A.2) on the invariant masses is removed for one pair of coloured particles. This situation depicted in equation (A.3) is termed the *Quasi-Multi-Regge kinematic limit.*

$$\text{(A.3)}$$

Such components with leading contributions in the QMRK limit (and therefore NLL contributions in the MRK limit) are included in the current predictions. We do not yet have the virtual corrections to the photon impact current in equation (A.1), which is needed to regulate the IR gluon singularities in the impact current of equation (A.3). Therefore, the impact current of equation (A.3) is used only when the quark and gluon are in separate jets, such that it belongs to the 3-jet (or more) contribution.

There are yet more complicated contributions from QMRK entering at four jets, in particular the emission of a photon from a central $q\bar{q}$ pair as illustrated in equation (A.4):

$$\text{(A.4)}$$

The central vertex is extracted from full amplitudes as detailed in reference [38] for the case of W-emission. A further complication in the present case of photon production is that for processes with more than one quark line, the photon can couple to all quark lines, and the interference between insertions on any line must be taken into account. Each such interference generates separate momenta entering the resummation, since the t-channel momenta differ depending on whether the photon is emitted from an impact current or from a central emission vertex. Such interference is fully taken into account in HEJ as described in reference [45] in the case of Z-production.

A.3 Resummation

The simplicity of both the real and virtual corrections in the MRK and QMRK limit allow for all-order results to be obtained within this approximation. The reliance on the asymptotic

MRK limit of the amplitudes within BFKL theory, and the ensuing kinematic simplification to a dependence on 2-dimensional transverse momentum only, followed by a leading logarithmic accurate approximation to the phase space, allows for the fully inclusive all-order resummation of the emissions analytically through the BFKL [37] equation.[7]

The milder approximations and added complexity of the Lorentz invariant amplitudes in HEJ means that the phase space integrations have to be done numerically for each multiplicity, just as in the case of the full QCD amplitudes. Each multiplicity is integrated over explicitly. This has the obvious benefit over analytic resummation studies of allowing for the implementation of phase space cuts (e.g. jet vetos) that are crucial for this study. Technically, the all-order results are constructed using elements from the complexity of each of the references [38, 45, 51].

On top of the leading logarithms (denoted by LL) and the leading logarithmic corrections to all the sub-leading channels (denoted LL^+) HEJ includes for this calculation full matching of the Born amplitudes with up to 5 jets. The higher jet rates normally associated with high-energy corrections are here suppressed because of the central jet veto. In fact, the 3-jet contribution is less than 20% of the cross section across all $m_{j_1 j_2}$, and the 4 and 5 jet contributions are at the level of 5% level and less than 1% respectively.[8] This ensures that for most of the cross section (namely for the two-jet rate), $m_{j_1 j_2}$ will be a good estimate for $\sqrt{s}$ especially for large $m_{j_1 j_2}$.

B Perturbative stability including subleading effects

Given the large variation in the perturbative spectrum between fixed leading order and fixed next-to-leading order, and of its own accord, it is interesting to study the perturbative stability in the spectrum predicted with HEJ when taking into account the sub-leading channels described in appendix A.2. The 3-jet component of these (as in equation (A.3)) are channels that also enter at NLO, whereas the 4-jet component (as in equation (A.4)) would enter at NNLO.

Figure 6 compares the QCD component of $pp \to \gamma$+dijets within the cuts of the current study (table 2) calculated with HEJ at pure leading-logarithmic accuracy (LL), and including also the sub-leading channels of the quasi-multi-Regge kinematic limit (LL^+). The normalisation of both have been matched to NLO by calculating the cross section of the expansion of LL and LL^+ to the same accuracy $O(\alpha_s^3 \alpha)$ as NLO, and multiplying the resummed distribution by the ratio of fixed order to the expanded result. This procedure ensures NLO precision of the cross section and logarithmic accuracy of the distribution. The differences between LL and LL^+ are less than 20% and relatively uniform across $m_{j_1 j_2}$. We conclude that the distribution is perturbatively stable against the changes studied at sub-leading logarithmic order. The systematic treatment of the $\log(s)$ corrections to all orders has stabilised the perturbative expansion.

For completion, we compare in figure 7 $d\sigma/dm_{j_1 j_2}$ for full QCD NLO, and for the expansions of LL and LL^+ to $\alpha_s^3 \alpha$. We note that LL^+ is closer to the full NLO than LL

---

[7]The understanding of the factorisation of amplitudes is currently being pushed beyond even NLL [54, 55].

[8]The fact that the $\sigma_{3j}/\sigma_{2j} \approx \sigma_{4j}/\sigma_{3j} \approx \sigma_{5j}/\sigma_{4j}$ can be understood as the combined result of the central jet veto and the NLL contribution of unordered emissions, see appendix A.2.
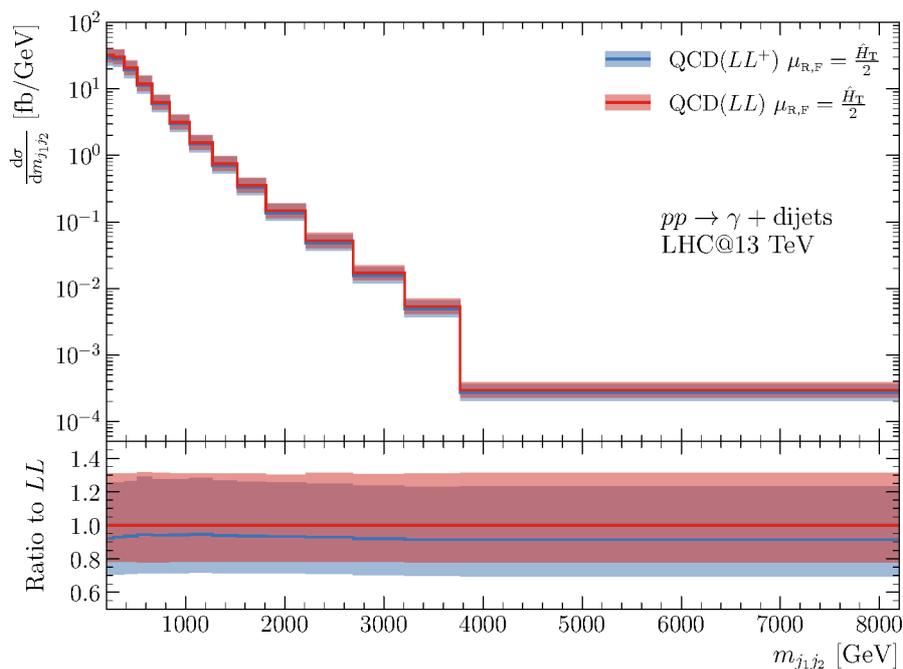
Figure 6. $d\sigma/dm_{j_1j_2}$ calculated with pure LL and including the sub-leading effects described in appendix A.2. The results were obtained using $\mu_R = \mu_F = \hat{H}_T/2$ and the cross section is in each case matched to NLO.
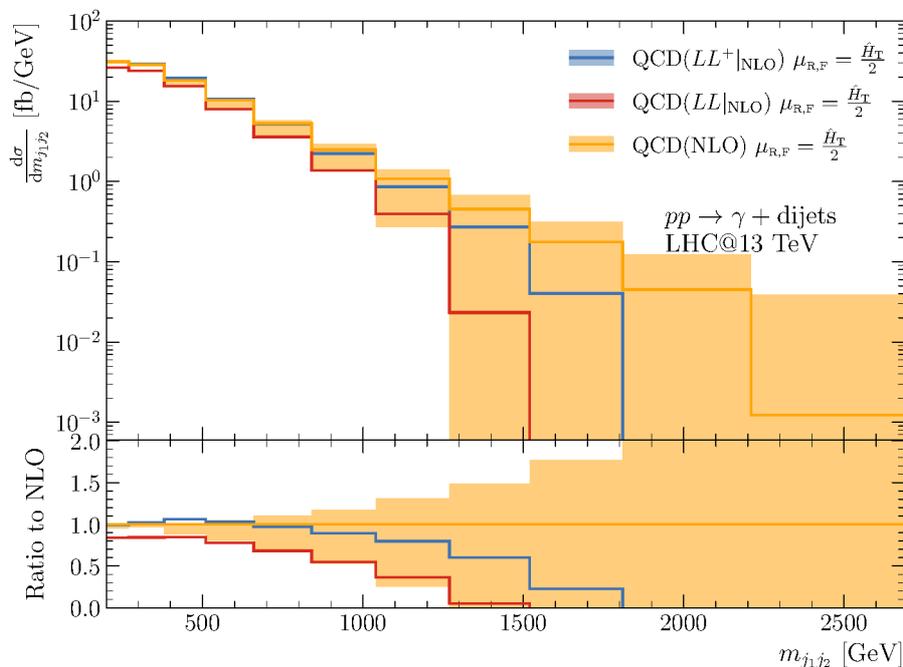

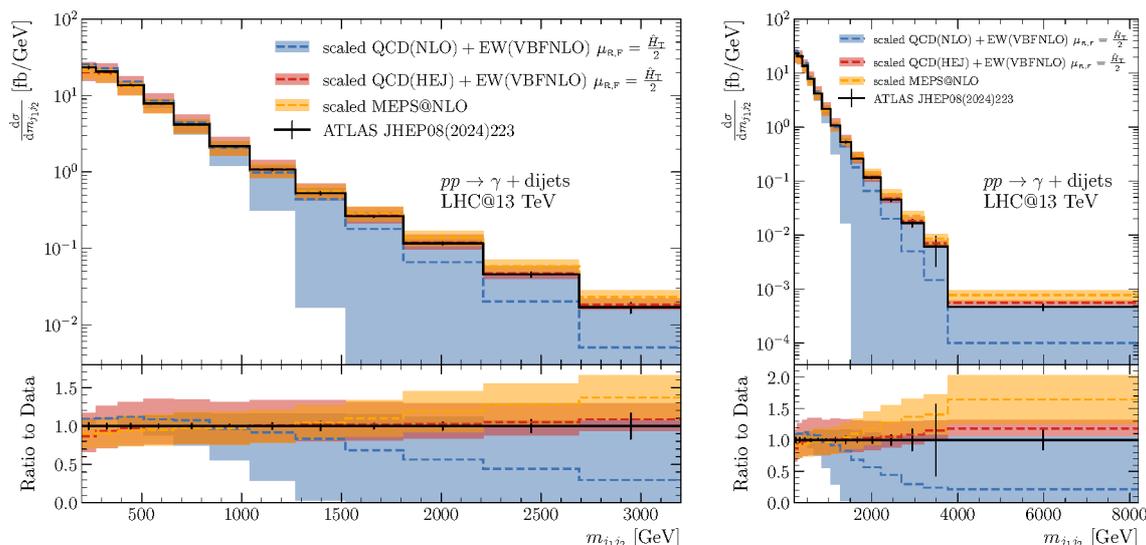**Figure 7.** $d\sigma/dm_{j_1j_2}$ for full QCD NLO and LL and LL^+ expanded to $\alpha_s^3\alpha$.

Figure 8. $d\sigma/dm_{j_1j_2}$ for scaled NLO, HEJ, MEPS@NLO and data, see table 3 for the scaling factors and χ^2/dof obtained.

for all $m_{j_1j_2}$, and all three descriptions turn negative for large $m_{j_1j_2}$. It may at first be surprising that the full NLO and LL or LL^+ terminated at order $\alpha_s^3\alpha$ do not converge at increasing $m_{j_1j_2}$. This is caused by sub-leading effects — the resummation essentially controls the slope of the curve but not the offset in $m_{j_1j_2}$.

C   Plots with MEPS@NLO

We present on figure 8 the same results as in figure 5 but with the results of MEPS@NLO added. The results of MEPS@NLO were obtained from the HEPData [56] entry of the ATLAS [2] study.

D   Perturbative results for renormalisation and factorisation scale $\mu = m_{j_1j_2}$

A natural choice for the factorisation and renormalisation scale even for large $m_{j_1j_2}$ is based on the transverse momenta of jets and the photon. Indeed, in the MRK limit, the t-channel factorisation discussed in appendix A connects independent components of the amplitude with t-type momenta, where in the MRK limit $|t| \to p_t^2$. Nevertheless, we have seen that the perturbative results obtained at NLO (or the NLO truncation of HEJ) is perturbatively unstable with the scale choice $\hat{H}_T/2$.

We will here investigate another scale choice. Having identified the $\log(s)$ as a source of problems for the fixed-order perturbative description, it becomes natural to investigate the choice of $\mu_{R,F} = m_{j_1j_2}$. Figure 9 shows the QCD fixed-order LO and NLO predictions (with scale variation bands obtained by the standard 7-point scale variation). There appears to be better perturbative stability with this scale choice: the NLO central prediction is just at the edge of the LO scale variation band, and more importantly it remains positive for all
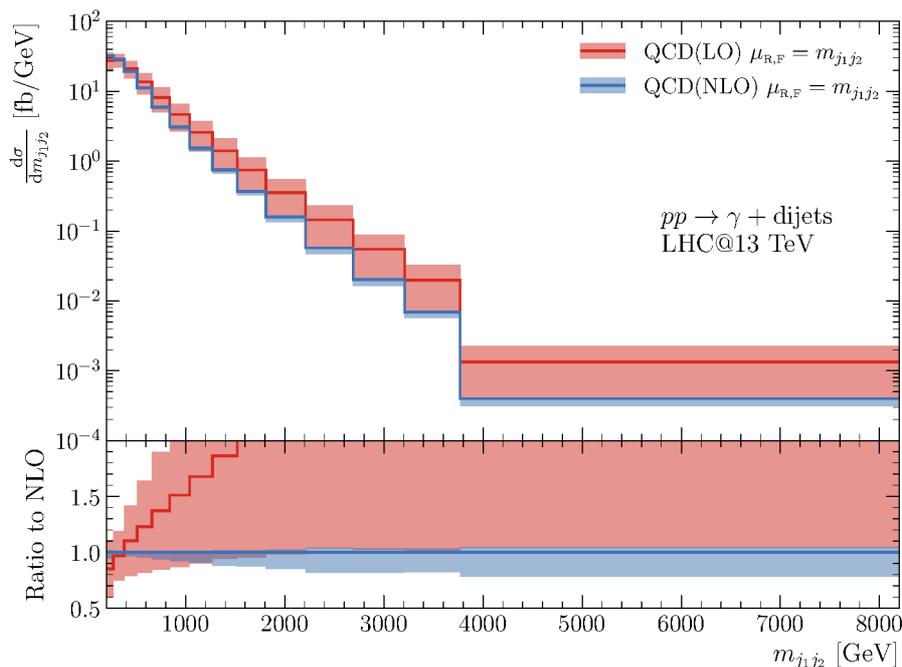
Figure 9. $d\sigma/dm_{j_1 j_2}$ for pure QCD at LO and at NLO calculated with $\mu_{\mathrm{R,F}} = m_{j_1 j_2}$.

$m_{j_1 j_2}$. The central NLO prediction is, however, close to the extreme of its scale variation band, which at least serves as a reminder that scale variation in itself is not necessarily a good proxy for estimating theory uncertainty. Figure 10 compares the NLO predictions for the two central scale choices of $\mu_{\mathrm{R,F}} = \hat{H}_T/2$ and $\mu_{\mathrm{R,F}} = m_{j_1 j_2}$. The difference between these two scales grows for increasing $m_{j_1 j_2}$ and so do the predictions for the cross section, and there is hardly any overlap of the scale variation bands. The interplay between effects from pdf and α_s is interesting — even if the α_s evaluation at the larger scale $m_{j_1 j_2}$ leads to a smaller α_s, the evaluation of the pdfs at the larger scale means the cross section is uniformly larger for the scale choice $\mu_{\mathrm{R,F}} = m_{j_1 j_2}$. In summary, choosing the scale $\mu_{\mathrm{R,F}} = m_{j_1 j_2}$ means that at least superficially the fixed-order perturbative predictions pass the standard test of perturbative stability, compared to the failure with $\mu_{\mathrm{R,F}} = \hat{H}_T/2$.

The investigation of a scale choice of $\mu_{\mathrm{R,F}} = m_{j_1 j_2}$ for the fixed-order QCD component is pushed yet further in figure 11 by adding the NLO VBF component to compare directly with data. The figure includes also the same prediction from HEJ presented on figure 4. The behaviour of the summed NLO predictions for the QCD($\mu_{\mathrm{R,F}} = m_{j_1 j_2}$) and EW($\mu_{\mathrm{R,F}} = \hat{H}_T/2$) components is surprisingly similar to that obtained with HEJ, even if the spectrum is a little less steeply falling in $m_{j_1 j_2}$. We remind the reader that HEJ systematically sums perturbative corrections of $\alpha_s \log(s)$ to all orders, which influence exactly the behaviour at large $\log(s)$ (and therefore at large $\log(m_{j_1 j_2})$). Even if the shape of the NLO obtained with the larger scale choice is better than that obtained with $\mu_{\mathrm{R,F}} = \hat{H}_T/2$, the normalisation is still significantly above data.
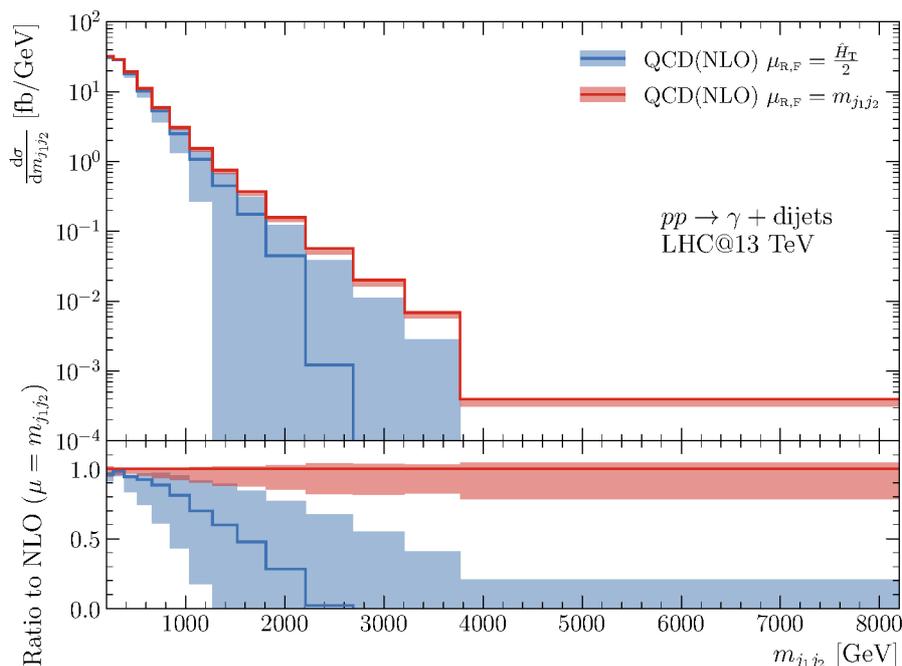
– 17 –

Figure 10. $d\sigma/dm_{j_1 j_2}$ for QCD NLO with $\mu_{\mathrm{R,F}} = \hat{H}_T/2$ and $\mu_{\mathrm{R,F}} = m_{j_1 j_2}$. The scale variation bands for central scale choice of $\mu_{\mathrm{R,F}} = \hat{H}_T/2$ and $\mu_{\mathrm{R,F}} = m_{j_1 j_2}$ overlap only for small $m_{j_1 j_2}$, and the central line for $\mu_{\mathrm{R,F}} = m_{j_1 j_2}$ is close to the extreme of the scale variation band around this central value. The central value for $\mu_{\mathrm{R,F}} = \hat{H}_T/2$ is negative for large $m_{j_1 j_2}$.
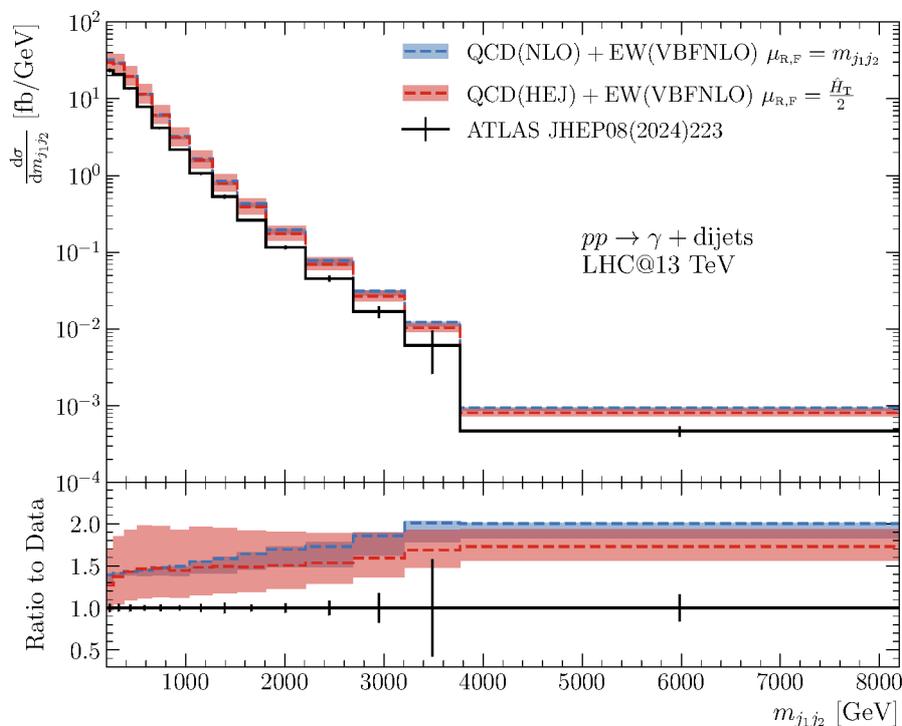
Figure 11. $d\sigma/dm_{j_1 j_2}$ for NLO QCD+EWK with $m_{j_1 j_2}$ and HEJ+EWK ($\hat{H}_T/2$) and data.
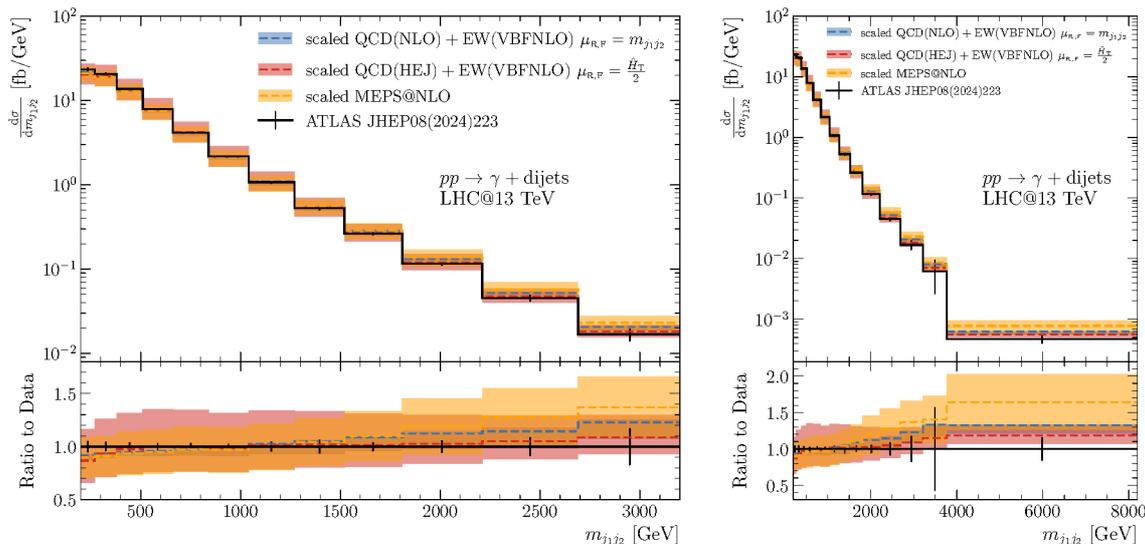
Figure 12. $d\sigma/dm_{j_1 j_2}$ for scaled NLO $\mu_{\mathrm{R,F}} = m_{j_1 j_2}$, HEJ, MEPS@NLO and data.

Prediction	Scaling factor σ	χ^2_σ/dof	Scaling factor $\chi^2_{\min}$	$\chi^2_{\min}/dof$
QCD(NLO)+EW(NLO)	0.755	16.3	0.810	14.3
MEPS@NLO	0.832	5.03	0.779	3.18
QCD(NLO, $\mu_{\mathrm{R,F}} = m_{j_1 j_2}$)+EW(NLO)	0.694	2.50	0.662	1.54
QCD(HEJ)+EW(NLO)	0.716	1.25	0.689	0.670

Table 4. Scaling factors for normalising the cross section and for minimising χ^2 in the description of the distribution.

Figure 12 compares the NLO prediction normalised to minimise the χ^2 with the scaling factor listed in table 4. Also shown are the predictions from MEPS@NLO (from the ATLAS paper [2]) and HEJ already presented in figure 5.

The minimum χ^2/dof obtained is just twice that obtained with HEJ and reduced by an order of magnitude compared to the result obtained with $\mu_{\mathrm{R,F}} = \hat{H}_T/2$.

Finally, to further indicate that the resummation in HEJ of the $\log(s)$ perturbative corrections stabilises the perturbative prediction, figure 13 shows the resummed predictions obtained with the two scales choices $\mu_{\mathrm{R,F}} = \hat{H}_T/2$ and $\mu_{\mathrm{R,F}} = m_{j_1 j_2}$. We emphasise again that especially in the approach with the amplitudes factorised into high-energy components, there is no physical argument for a renormalisation scale of $\mu_{\mathrm{R,F}} = m_{j_1 j_2}$. Nevertheless, it is interesting that we observe an overlap between the scale variation bands. Unsurprisingly, the difference between the predictions increases with increasing $m_{j_1 j_2}$ as the scale of α_s is influenced.

Data Availability Statement. This article has no associated data or the data will not be deposited.

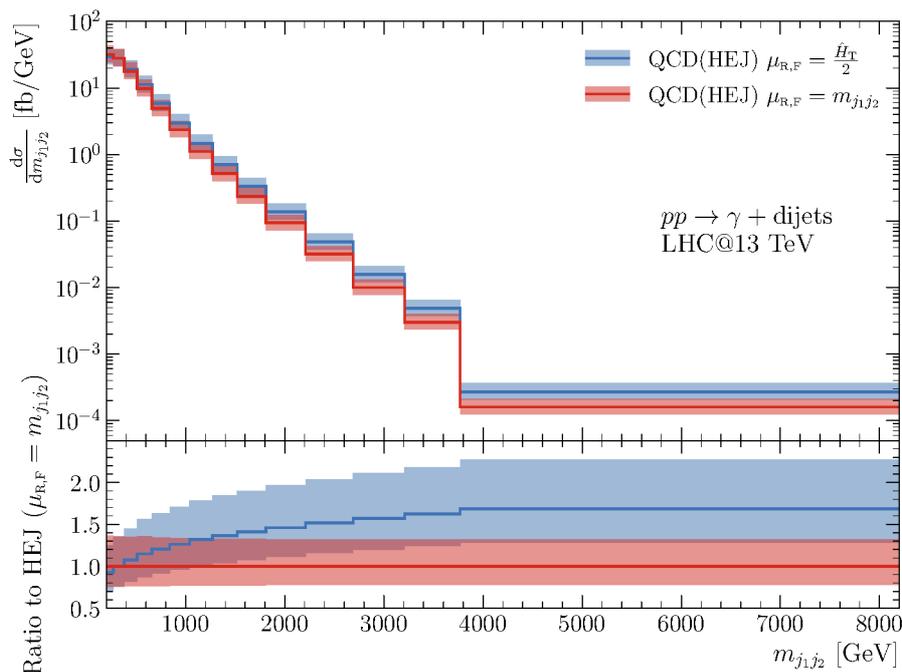**Code Availability Statement.** This article has associated code in a code repository. https://hej.hepforge.org.

Figure 13. $\mathrm{d}\sigma/\mathrm{d}m_{j_1 j_2}$ for pure QCD HEJ with $\mu_{\mathrm{R,F}} = \hat{H}_T/2$ and $\mu_{\mathrm{R,F}} = m_{j_1 j_2}$.

References

[1] ATLAS collaboration, *Standard Model Summary Plots June 2024*, ATL-PHYS-PUB-2024-011, CERN, Geneva (2024).

[2] ATLAS collaboration, *Differential cross-sections for events with missing transverse momentum and jets measured with the ATLAS detector in 13 TeV proton-proton collisions*, *JHEP* **08** (2024) 223 [arXiv:2403.02793] [INSPIRE].

[3] ATLAS collaboration, *Measurement of isolated-photon plus two-jet production in pp collisions at $\sqrt{s} = 13$ TeV with the ATLAS detector*, *JHEP* **03** (2020) 179 [arXiv:1912.09866] [INSPIRE].

[4] S. Badger et al., *Isolated photon production in association with a jet pair through next-to-next-to-leading order in QCD*, *JHEP* **10** (2023) 071 [arXiv:2304.06682] [INSPIRE].

[5] S. Hoeche, F. Krauss, M. Schonherr and F. Siegert, *QCD matrix elements + parton showers: the NLO case*, *JHEP* **04** (2013) 027 [arXiv:1207.5030] [INSPIRE].

[6] S. Catani, M. Fontannaz, J.P. Guillet and E. Pilon, *Isolating Prompt Photons with Narrow Cones*, *JHEP* **09** (2013) 007 [arXiv:1306.6498] [INSPIRE].

[7] M. Balsiger, T. Becher and D.Y. Shao, *Non-global logarithms in jet and isolation cone cross sections*, *JHEP* **08** (2018) 104 [arXiv:1803.07045] [INSPIRE].

[8] T. Becher, S. Favrod and X. Xu, *QCD anatomy of photon isolation*, *JHEP* **01** (2023) 005 [arXiv:2208.01554] [INSPIRE].

[9] T. Becher, M. Neubert, D.Y. Shao and M. Stillger, *Factorization of non-global LHC observables and resummation of super-leading logarithms*, *JHEP* **12** (2023) 116 [arXiv:2307.06359] [INSPIRE].

[10] P. Böer et al., *Resummation of Glauber phases in non-global LHC observables for large N_c*, *JHEP* **08** (2024) 036 [arXiv:2407.01691] [INSPIRE].

[11] T. Becher et al., *Super-leading logarithms in $pp \to 2$ jets*, *JHEP* **01** (2025) 171 [arXiv:2411.12742] [INSPIRE].

[12] P. Böer et al., *Renormalization-group improved resummation of super-leading logarithms*, *JHEP* **08** (2024) 035 [arXiv:2405.05305] [INSPIRE].

[13] J.R. Forshaw, A. Kyrieleis and M.H. Seymour, *Super-leading logarithms in non-global observables in QCD*, *JHEP* **08** (2006) 059 [hep-ph/0604094] [INSPIRE].

[14] J.R. Forshaw, A. Kyrieleis and M.H. Seymour, *Super-leading logarithms in non-global observables in QCD: colour basis independent calculation*, *JHEP* **09** (2008) 128 [arXiv:0808.1269] [INSPIRE].

[15] R. Ángeles Martínez et al., *Soft gluon evolution and non-global logarithms*, *JHEP* **05** (2018) 044 [arXiv:1802.08531] [INSPIRE].

[16] A. Banfi, F.A. Dreyer and P.F. Monni, *Higher-order non-global logarithms from jet calculus*, *JHEP* **03** (2022) 135 [arXiv:2111.02413] [INSPIRE].

[17] T. Becher et al., *Factorization Restoration through Glauber Gluons*, *Phys. Rev. Lett.* **134** (2025) 061901 [arXiv:2408.10308] [INSPIRE].

[18] C. Bierlich et al., *Robust independent validation of experiment and theory: Rivet version 4 release note*, *SciPost Phys. Codeb.* **36** (2024) 1 [arXiv:2404.15984] [INSPIRE].

[19] J.R. Andersen, T. Binoth, G. Heinrich and J.M. Smillie, *Loop induced interference effects in Higgs Boson plus two jet production at the LHC*, *JHEP* **02** (2008) 057 [arXiv:0709.3513] [INSPIRE].

[20] A. Bredenstein, K. Hagiwara and B. Jager, *Mixed QCD-electroweak contributions to Higgs-plus-dijet production at the LHC*, *Phys. Rev. D* **77** (2008) 073004 [arXiv:0801.4231] [INSPIRE].

[21] L.J. Dixon and Y. Sofianatos, *Analytic one-loop amplitudes for a Higgs boson plus four partons*, *JHEP* **08** (2009) 058 [arXiv:0906.0008] [INSPIRE].

[22] SHERPA collaboration, *Event Generation with Sherpa 2.2*, *SciPost Phys.* **7** (2019) 034 [arXiv:1905.09127] [INSPIRE].

[23] F. Buccioni et al., *OpenLoops 2*, *Eur. Phys. J. C* **79** (2019) 866 [arXiv:1907.13071] [INSPIRE].

[24] M. Cacciari, G.P. Salam and G. Soyez, *The anti-k_t jet clustering algorithm*, *JHEP* **04** (2008) 063 [arXiv:0802.1189] [INSPIRE].

[25] M. Cacciari and G.P. Salam, *Dispelling the N^3 myth for the k_t jet-finder*, *Phys. Lett. B* **641** (2006) 57 [hep-ph/0512210] [INSPIRE].

[26] NNPDF collaboration, *Parton distributions from high-precision collider data*, *Eur. Phys. J. C* **77** (2017) 663 [arXiv:1706.00428] [INSPIRE].

[27] A. Buckley et al., *LHAPDF6: parton density access in the LHC precision era*, *Eur. Phys. J. C* **75** (2015) 132 [arXiv:1412.7420] [INSPIRE].

[28] PDF4LHC WORKING GROUP collaboration, *The PDF4LHC21 combination of global PDF fits for the LHC Run III*, *J. Phys. G* **49** (2022) 080501 [arXiv:2203.05506] [INSPIRE].

[29] C.F. Berger et al., *Next-to-Leading Order QCD Predictions for W+3-Jet Distributions at Hadron Colliders*, *Phys. Rev. D* **80** (2009) 074036 [arXiv:0907.1984] [INSPIRE].

[30] C.F. Berger et al., *Precise Predictions for W + 4 Jet Production at the Large Hadron Collider*, *Phys. Rev. Lett.* **106** (2011) 092001 [arXiv:1009.2338] [INSPIRE].

[31] H. Ita et al., *Precise Predictions for Z + 4 Jets at Hadron Colliders*, *Phys. Rev. D* **85** (2012) 031501 [arXiv:1108.2229] [INSPIRE].

[32] Z. Bern et al., *Next-to-Leading Order W + 5-Jet Production at the LHC*, *Phys. Rev. D* **88** (2013) 014025 [arXiv:1304.1253] [INSPIRE].

[33] F. Caola, F.A. Dreyer, R.W. McDonald and G.P. Salam, *Framing energetic top-quark pair production at the LHC*, *JHEP* **07** (2021) 040 [arXiv:2101.06068] [INSPIRE].

[34] V.S. Fadin, E.A. Kuraev and L.N. Lipatov, *On the Pomeranchuk Singularity in Asymptotically Free Theories*, *Phys. Lett. B* **60** (1975) 50 [INSPIRE].

[35] E.A. Kuraev, L.N. Lipatov and V.S. Fadin, *Multiregge processes in the Yang-Mills theory*, *Sov. Phys. JETP* **44** (1976) 443 [INSPIRE].

[36] E.A. Kuraev, L.N. Lipatov and V.S. Fadin, *The Pomeranchuk singularity in nonabelian gauge theories*, *Sov. Phys. JETP* **45** (1977) 199.

[37] I.I. Balitsky and L.N. Lipatov, *The Pomeranchuk Singularity in Quantum Chromodynamics*, *Sov. J. Nucl. Phys.* **28** (1978) 822 [INSPIRE].

[38] J.R. Andersen et al., *Combined subleading high-energy logarithms and NLO accuracy for W production in association with multiple jets*, *JHEP* **04** (2021) 105 [arXiv:2012.10310] [INSPIRE].

[39] B. Jager, *Next-to-leading order QCD corrections to photon production via weak-boson fusion*, *Phys. Rev. D* **81** (2010) 114016 [arXiv:1004.0825] [INSPIRE].

[40] J. Baglio et al., *Release note: VBFNLO 3.0*, *Eur. Phys. J. C* **84** (2024) 1003 [arXiv:2405.06990] [INSPIRE].

[41] Y.L. Dokshitzer, V.A. Khoze and T. Sjostrand, *Rapidity gaps in Higgs production*, *Phys. Lett. B* **274** (1992) 116 [INSPIRE].

[42] ATLAS collaboration, *Measurements of jet cross-section ratios in 13 TeV proton-proton collisions with ATLAS*, *Phys. Rev. D* **110** (2024) 072019 [arXiv:2405.20206] [INSPIRE].

[43] GRIDPP collaboration, *GridPP: development of the UK computing Grid for particle physics*, *J. Phys. G* **32** (2006) N1 [INSPIRE].

[44] D. Britton et al., *GridPP: the UK grid for particle physics*, *Phil. Trans. Roy. Soc. Lond. A* **367** (2009) 2447 [INSPIRE].

[45] J.R. Andersen, J.J. Medley and J.M. Smillie, *Z/γ* plus multiple hard jets in high energy collisions*, *JHEP* **05** (2016) 136 [arXiv:1603.05460] [INSPIRE].

[46] V. Del Duca, *An introduction to the perturbative QCD pomeron and to jet physics at large rapidities*, hep-ph/9503226 [INSPIRE].

[47] V. Del Duca, *Equivalence of the Parke-Taylor and the Fadin-Kuraev-Lipatov amplitudes in the high-energy limit*, *Phys. Rev. D* **52** (1995) 1527 [hep-ph/9503340] [INSPIRE].

[48] V. Del Duca, A. Frizzo and F. Maltoni, *Factorization of tree QCD amplitudes in the high-energy limit and in the collinear limit*, *Nucl. Phys. B* **568** (2000) 211 [hep-ph/9909464] [INSPIRE].

[49] J.R. Andersen and J.M. Smillie, *Constructing All-Order Corrections to Multi-Jet Rates*, *JHEP* **01** (2010) 039 [arXiv:0908.2786] [INSPIRE].

[50] J.R. Andersen and J.M. Smillie, *The factorisation of the t-channel Pole in Quark-Gluon Scattering*, *Phys. Rev. D* **81** (2010) 114021 [arXiv:0910.5113] [INSPIRE].

[51] J.R. Andersen and J.M. Smillie, *Multiple Jets at the LHC with High Energy Jets*, *JHEP* **06** (2011) 010 [arXiv:1101.5394] [INSPIRE].

[52] V. Del Duca and E.W.N. Glover, *The High-energy limit of QCD at two loops*, *JHEP* **10** (2001) 035 [hep-ph/0109028] [INSPIRE].

[53] A.V. Bogdan, V. Del Duca, V.S. Fadin and E.W.N. Glover, *The Quark Regge trajectory at two loops*, *JHEP* **03** (2002) 032 [hep-ph/0201240] [INSPIRE].

[54] F. Buccioni, F. Caola, F. Devoto and G. Gambuti, *Investigating the universality of five-point QCD scattering amplitudes at high energy*, *JHEP* **03** (2025) 129 [arXiv:2411.14050] [INSPIRE].

[55] S. Abreu et al., *The two-loop Lipatov vertex in QCD*, *JHEP* **04** (2025) 161 [arXiv:2412.20578] [INSPIRE].

[56] E. Maguire, L. Heinrich and G. Watt, *HEPData: a repository for high energy physics data*, *J. Phys. Conf. Ser.* **898** (2017) 102006 [arXiv:1704.05473] [INSPIRE].

[57] *HEJ: High Energy Jets*, https://hej.hepforge.org